

Cold atoms in videotape micro-traps

C. D. J. Sinclair, J. A. Retter,* E. A. Curtis,† B. V. Hall,‡ I. Llorente Garcia, S. Eriksson, B. E. Sauer, and E. A. Hinds
*Blackett Laboratory, Imperial College,
 London, SW7 2BW, UK*

(Dated: September 4, 2018)

We describe an array of microscopic atom traps formed by a pattern of magnetisation on a piece of videotape. We describe the way in which cold atoms are loaded into one of these micro-traps and how the trapped atom cloud is used to explore the properties of the trap. Evaporative cooling in the micro-trap down to a temperature of $1 \mu\text{K}$ allows us to probe the smoothness of the trapping potential and reveals some inhomogeneity produced by the magnetic film. We discuss future prospects for atom chips based on microscopic permanent-magnet structures.

PACS numbers: 39.25.+k, 03.75.Be, 75.50.Ss

I. INTRODUCTION

Magnetic storage media provide a convenient way to prepare small magnetic structures that can be used to manipulate cold atoms. These include audiotape [1], floppy disks [2, 3, 4], videotape [5, 6], magneto-optical films [7, 8, 9], and hard disks [10]. Using standard lithographic techniques, it is also possible to make small patterns of current carrying wires for the same purpose [11, 12]. This has led to the concept of the atom chip, in which small structures are integrated on a substrate and used to control the motion and interactions of microscopic cold atom clouds. The atom chip presents opportunities for quantum coherent manipulation of atoms for quantum information processing or fundamental studies of quantum gases. It also creates a versatile miniaturised system ideal for manipulating cold atom clouds in a variety of applications such as magnetometry [13], interferometry [14] and miniature clocks [15, 16]. For a number of years it has been clear that permanent-magnet microstructures have a significant contribution to make to atom chips [17], since they have the possibility of making very tight atom traps with cloud sizes approaching 10 nm. So far, however, magnetic microstructures have only been used to control much larger macroscopic clouds.

In this paper we describe a permanent-magnet atom chip, an adaptation of the magnetic mirror described in reference [17], in which we prepare and manipulate small atom clouds with radial sizes down to 50 nm. The next section introduces the videotape and shows how periodic magnetisation can be used to trap atoms. Section III describes the design and structure of the videotape atom chip. The loading, cooling and trapping of atoms in a

videotape micro-trap are described in Section IV. In Section V we describe experiments to test our understanding of these micro-traps and to study the quality of the videotape. In the final section we discuss some of the future directions of permanent-magnet atom-chip experiments.

II. MAGNETIC MEDIA AND ATOM TRAPS

The basis of our micro-traps is a magnetic pattern written on videotape as illustrated in Fig. 1. As in the magnetic mirror we use a sinusoidal pattern, however, in this work we add a bias field to form an array of micro-traps. With magnetisation $M_0 \cos kx$ along the x direction, the magnetic field outside the film is

$$(B_x, B_y) = B_{sur} e^{-ky} (-\cos(kx), \sin(kx)). \quad (1)$$

For a film of thickness b , the field at the surface is

$$B_{sur} = \frac{1}{2} \mu_0 M_0 (1 - e^{-kb}). \quad (2)$$

Thus the potential energy of a weak-field-seeking atom increases exponentially as it approaches the mirror surface. This is how the atom is reflected.

The micro-traps appear when a bias field B_{bias} is superimposed in the x - y plane, as shown in Fig. 1. Near each trap the magnetic field has a quadrupole structure with a zero in the centre and a gradient of field strength given by

$$B' = kB_{bias}. \quad (3)$$

In order to suppress Majorana spin flips of the trapped atoms, we also apply an axial bias field B_z , which prevents the total field from going exactly to zero at the centre. For small-amplitude transverse oscillations this makes a harmonic trap with frequency

$$2\pi f_r = kB_{bias} \sqrt{\frac{\mu_B g_F m_F}{m B_z}}, \quad (4)$$

where $\mu_B g_F m_F$ is the usual factor in the Zeeman energy and m is the mass of the atom. The trap centres are

*Now at Laboratoire Charles Fabry de l'Institut d'Optique, UMR8501 du CNRS, 91403 Orsay Cedex, France.

†Electronic address: a.curtis@imperial.ac.uk

‡Now at Centre for Atom Optics and Ultrafast Spectroscopy, Swinburne University of Technology, Melbourne, Australia.

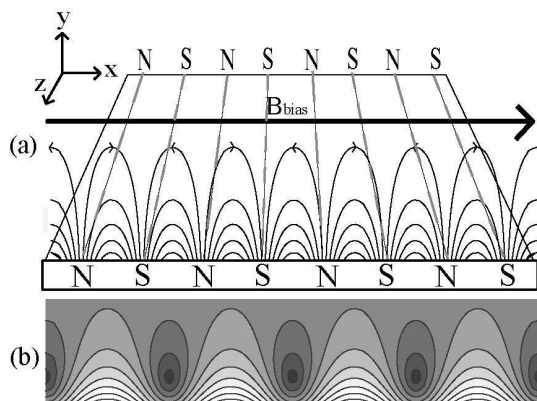


FIG. 1: (a) Magnetic field lines produced by the magnetised videotape. A uniform bias field is added to this to make an array of atom guides. (b) Contours of constant magnetic field strength. Circular contours enclose the lines of minimum field strength, where atoms are trapped.

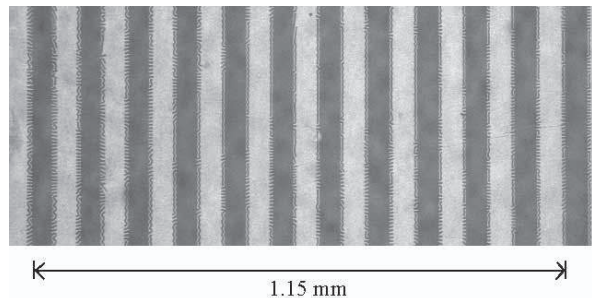


FIG. 2: Optical microscope image showing reversals of the magnetic field direction. These are revealed by a thin garnet film placed on the surface, viewed with polarised light through a crossed analyser.

formed at a distance y_{trap} from the surface, given by

$$y_{trap} = \frac{1}{k} \ln(B_{sur}/B_{bias}). \quad (5)$$

Ref. [17] provides further detail about permanent magnetic patterns and their corresponding fields.

III. VIDEOTAPE ATOM CHIP DESIGN

We have chosen to use videotape because it can store patterns with feature sizes down to a few micrometers using simple commercial recording equipment adapted in the laboratory. Videotape is designed to hold data reliably for long periods of time and has a high coercivity, making the magnetisation insensitive to the presence of the bias fields. The particular tape we use, Ampex 398 Betacam SP, has a $3.5 \mu\text{m}$ -thick magnetic layer containing iron-composite needles, 100 nm long with 10 nm radius, which are set in a glue and aligned parallel to the x direction. This film is supported by a polymer ribbon $11 \mu\text{m}$ thick. Since atom-trap experiments are con-

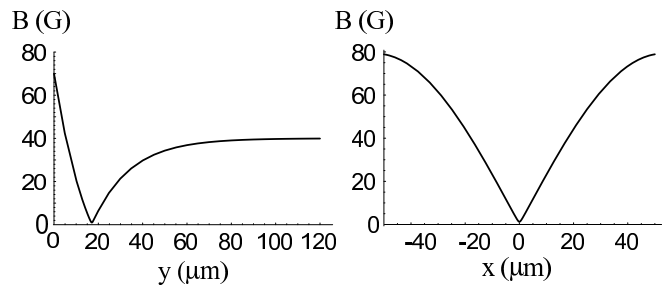


FIG. 3: Magnetic field strength plotted versus x and y going through the centre of a trap. Here we take bias fields of 40 G along x and 1 G along z . The videotape field has a strength of 110 G at the surface and the trap forms $17 \mu\text{m}$ away from the surface.

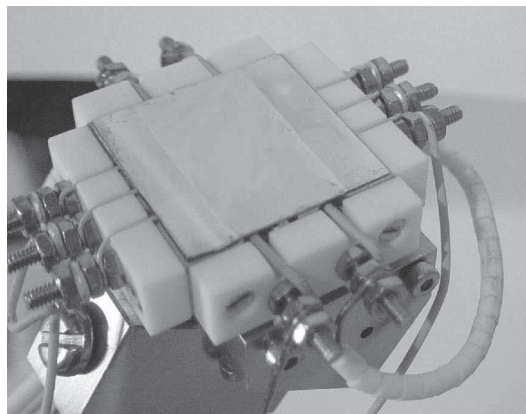


FIG. 4: The videotape atom chip assembly. The reflective surface of the chip is one inch square.

ducted in ultra-high vacuum conditions at a few times 10^{-11} Torr, the vacuum properties of the materials we use are important. Remarkably, this videotape has a very low outgassing rate at room temperature and is able to withstand baking at 120°C [18].

For the experiments described in this paper, the magnetic sine wave has a period of $106 \pm 2 \mu\text{m}$. We are able to observe this directly by placing a thin Faraday-rotating garnet film (Nd:Lu:Bi) on the surface and viewing it under a microscope with polarised light, as shown in Fig. 2. The accurate measurement of the period is achieved by counting a large number of these fringes.

We have measured that the field at the surface of the tape is 110 ± 10 G, as we discuss further in Section V. Taking this value together with typical bias fields $B_{bias} = 40$ G and $B_z = 1$ G, we calculate the expected trapping field strength shown in Fig. 3. For trapped ^{87}Rb atoms in the $|F = 2, m_F = 2\rangle$ sublevel of the ground state, the small-amplitude radial oscillation frequency is 30 kHz.

After recording, a piece of the videotape is glued to a glass coverslip $150 \mu\text{m}$ thick using a UHV-compatible epoxy (BYLAPOX 7285), as described in references [19, 20]. This is coated with a ~ 5 nm adhesion layer of chromium and ~ 400 nm of gold in order to make the

surface of the chip reflect 780 nm laser light. The purpose here is to allow the formation of a magneto-optical trap (MOT) by reflection [21] in order to collect and cool the atoms close to the videotape. The coverslip is then glued to a 1 inch square stainless-steel base to form the chip assembly shown in Fig. 4. Five wires insulated by a ceramic coating run underneath the coverslip through channels cut into the steel, ending on Macor terminal blocks. The three wires parallel to the z direction lie immediately below the coverslip and have $500 \mu\text{m}$ diameters. The central one of these, the “centre wire”, is used to transport cold atoms from the MOT into one videotape micro-trap, whilst the outer two form an rf antenna used subsequently for evaporative cooling of the atoms. Two larger, 1 mm-diameter wires run along x and pass below the centre wire. These are separated by 8.5 mm. Currents in these allow the trap to be closed off at its ends by making a field that rises to a maximum in the z direction above each wire. The whole assembly is mounted in the high-vacuum chamber on a flange that allows translation under vacuum in any direction.

IV. LOADING A MICRO-TRAP

A double MOT system delivers cold ^{87}Rb atoms to the atom chip assembly. The first MOT, in an auxiliary chamber, is a low-velocity intense source (LVIS)[22] with three retro-reflected laser beams. The Rb atoms are provided by a resistively-heated dispenser that increases the pressure to $\sim 1 \times 10^{-9}$ Torr. The LVIS delivers a ~ 15 m/s beam of cold atoms into the main vacuum chamber through a 6 mm-long, 1 mm-diameter aperture 30 cm away from the atom chip. The second MOT, in the main chamber, is formed by four independent laser beams, two of which we reflect from the surface of the chip. The magnetic quadrupole field is provided by coils located outside the chamber. When this MOT is loaded by the LVIS source for 20 s, $\sim 3 \times 10^8$ atoms are collected at a temperature of $\sim 150 \mu\text{K}$ and at a distance of 4 mm from the chip. The pressure in this chamber is too low to register on the ionisation gauge, which cuts out below 3×10^{-11} Torr. The MOT lifetime exceeds 50 s.

Once the MOT has been filled, the dispenser and laser beams of the LVIS are turned off and the cloud is moved to 1.5 mm from the chip by ramping up an external bias field of ~ 4 G. At this point, the red-detuning of the laser from the $\text{D2}(F = 2 \rightarrow 3)$ cooling transition is increased over 14 ms from -15 MHz to -45 MHz. This cools the cloud to $\sim 50 \mu\text{K}$. Next, the MOT is switched off (both the light and the field) and a uniform field is applied in order to optically pump using σ^+ light on the $\text{D2}(F = 2 \rightarrow 2)$ transition for $400 \mu\text{s}$. This transfers the atoms into the $|F = 2, m_F = 2\rangle$ weak-field-seeking state. Approximately 3×10^7 of these atoms are then recaptured in a purely magnetic trap, formed by passing 15 A through the centre wire and imposing a 14 G field along x . The efficiency of transfer from the MOT to the mag-

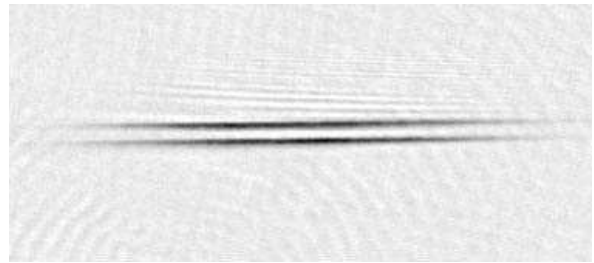


FIG. 5: Double image of atoms in a single videotape micro-trap. Dark areas correspond to regions of maximum absorption. Image area is $3.4 \text{ mm} \times 1.5 \text{ mm}$.

netic trap is particularly sensitive to the way in which the laser frequency is swept to larger detuning.

The bias field is immediately ramped up to 44 G over 100 ms, which increases the trap depth, compresses the cloud and moves it to $160 \mu\text{m}$ from the surface (where the field of the videotape is still negligible). This transfer heats the cloud adiabatically, increasing the elastic collision rate to $\sim 20 \text{ s}^{-1}$, which is sufficient to start evaporative cooling. The field at the centre of this trap is $\sim 500 \text{ mG}$, giving a radial oscillation frequency of 1.1 kHz, while the axial frequency is 15 Hz. In order to drive the evaporation, the rf field is now applied and its frequency is swept for 6 seconds according to $f = (30 e^{-t} + 3.9) \text{ MHz}$, where t is in seconds. This cools the cloud to $10 \mu\text{K}$. Leaving the rf field on at 3.9 MHz, we continue to evaporate by reducing the centre-wire current and the bias field over 4 s. This gradually brings the cloud close to the surface, into a region where the field of the videotape becomes comparable with the bias field. Finally, the wire current is ramped down to zero, leaving atoms confined solely by the videotape micro-trap. After this phase of compression and additional cooling there are a few times 10^5 atoms in the micro-trap at a temperature of $\sim 10 \mu\text{K}$. When lower temperatures than this are required, we make a second stage of rf evaporation that takes place entirely in the micro-trap.

The atoms are imaged by optical absorption, using a single pulse of light (typically $40 \mu\text{s}$ long), tuned to the $\text{D2}(F = 2 \rightarrow 3)$ transition. A CCD camera records the image of the cloud, formed at unit magnification by a high-quality achromatic doublet lens. The imaging beam makes an angle of $\sim 10^\circ$ to the gold surface in order to give two images: the cloud and its reflection in the mirror. This provides a simple measure of the distance between the atoms and the surface. Figure 5 shows the image of 2×10^5 atoms at $20 \mu\text{K}$, held in a $15 \text{ Hz} \times 4.7 \text{ kHz}$ trap, $55 \mu\text{m}$ from the surface of the videotape.

V. EXPERIMENTS

Having now trapped the atoms, our first experiment is to check the exponential law for the strength of the videotape field given in Eq.(1) and to measure the sur-

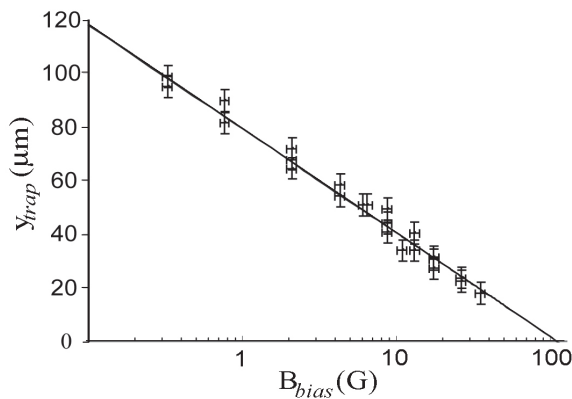


FIG. 6: Logarithmic dependence of atom-surface distance on the applied bias field. The intercept at zero height measures the field at the surface of the chip.

face field B_{sur} . According to Eq.(5), the distance between the trap and the surface, y_{trap} , should be linearly proportional to $\ln(B_{bias})$, with a slope of $1/k$ and an intercept on $y_{trap} = 0$ of $B_{bias} = B_{sur}$. Figure 6 shows measurements of y_{trap} for a variety of bias fields. These distances, to which we assign an uncertainty of $\pm 4 \mu\text{m}$ are derived from the separation measured between the centres of the two cloud images. The uncertainty in B_{bias} is a 7% calibration error. Our measurements confirm the exponential field decay of Eq.(1) and yield a value of $110 \pm 10 \text{ G}$ for B_{sur} . This is approximately half the maximum possible value given by Eq.(2) with $\mu_0 M_0$ equal to the saturated magnetisation, 2.3 kG. The result is not surprising since our method of recording was to monitor the playback signal and to set the current in the record head just below the level where any distortion was evident.

The second experiment is to investigate the frequencies of the micro-trap. In the axial direction, the restoring force is small enough that we can see oscillations of the cloud directly on the CCD camera. Typical axial frequencies are in the range 5 – 20 Hz. Figure 7 shows the centre-of-mass oscillation of a $1 \mu\text{K}$ cloud with an initial displacement of $100 \mu\text{m}$. The damping of this oscillation is due primarily to the collisional coupling into other degrees of freedom, with relatively little effect from the slight anharmonicity of the trap.

Radial oscillation cannot be observed in the same direct way because the frequency is too high. Moreover, the radial size of the cloud is far smaller than one pixel of the camera: a 30 kHz trap at $1 \mu\text{K}$, gives a cloud radius of 52 nm. Instead, we add a modulation $\delta B_{bias} \cos(2\pi ft)$ to the bias field, which shakes the trap in the radial direction. When the frequency f coincides with the radial oscillation frequency f_r , the cloud is heated. Once again, the collisions within the gas couple the motional degrees of freedom, allowing us to detect the radial heating through the corresponding increase in the length of the cloud. The inset in Fig. 8 shows the cloud temper-

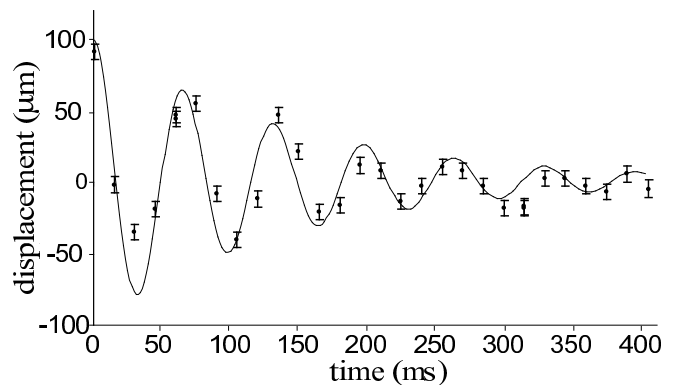


FIG. 7: Oscillations of the atom cloud in the axial direction. Each point involves a new realization of the experiment with a suitably chosen time delay before measuring the position of the cloud. The line is a damped sine wave intended to guide the eye.

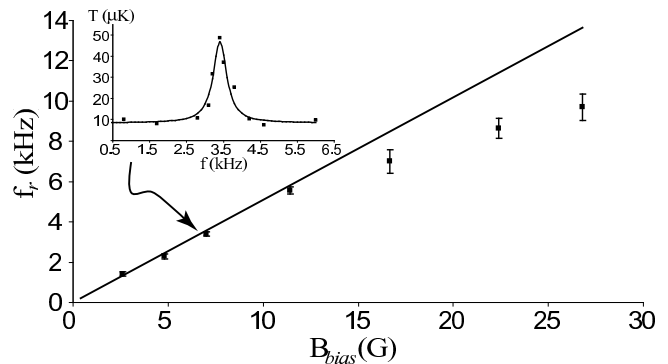


FIG. 8: Radial trap frequency versus applied bias field. Solid line: harmonic approximation given in Eq. 4. Data points: Measured radial trap frequencies. Inset: Typical radial excitation spectrum.

ature versus f , as measured by its length after applying the modulation for 5 s. The radial resonance is seen as a dramatic increase in the temperature. The main graph in Fig. 8 shows these resonance frequencies versus bias field. The solid line is the harmonic frequency given by Eq. 4 with $B_z = 2 \text{ G}$, corresponding to the axial field used in these experiments. At low bias field, we see good agreement between this formula and the measured radial frequency. With a stronger bias, the radial frequency lies below the prediction of Eq. 4 (and the resonances are broader). We believe this is due to the compression of the cloud, which occurs when B_{bias} is increased after loading the micro-trap. This increases the initial temperature and expands the cloud out of the central region where the harmonic approximation is valid. Here the potential is more linear, as one can see in Fig. 3 (indeed, the harmonic region is almost invisible on the scale of Fig. 3), giving rise to a lower oscillation frequency and a broadening of the resonance feature.

Our final experiment uses the cold atoms to probe the magnetic smoothness of the videotape. Figure 9 shows

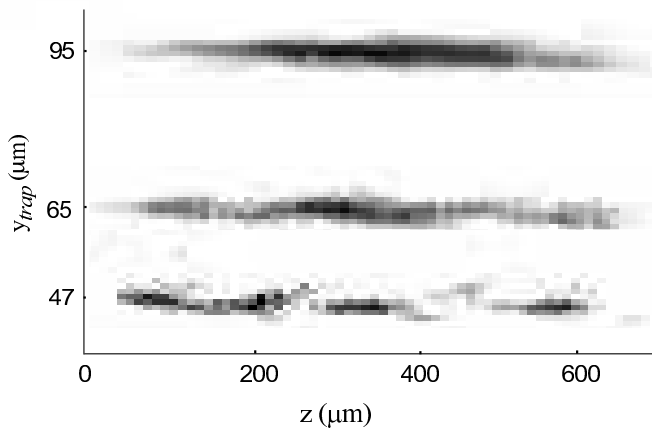


FIG. 9: Density distribution of trapped atom clouds at three different heights above the videotape.

the density distribution of a $1 \mu\text{K}$ cloud at three different distances from the surface. The cloud has a smooth profile at a distance of $100 \mu\text{m}$, but develops structure as it approaches the surface. This is reminiscent of the structure observed near a wire (see [23], [24], and references therein), which is caused by an alternating magnetic field in the z direction due to a transverse component of the current density in the wire. The structure we see here is also caused by an alternating magnetic field along the z direction, although of course there are no currents flowing in the videotape. In this case, it is an alternating component of magnetization along z that causes the unwanted magnetic field through an effective current density $j_x = \partial M_z / \partial y$.

In order to discover how this fluctuating z component of magnetisation comes about, we have studied a piece of tape taken from the same cassette as the tape. Figure 10 shows the surface topography of this sample as measured by an atomic force microscope. The greyscale indicates the height of the tape measured over an area of $100 \mu\text{m} \times 50 \mu\text{m}$. Below that is a graph showing the typical height profile along a line. These images reveal some small height variations over transverse lengths of tens of micrometers, which are only due to the failure of the tape to lie flat. In addition, however, we see some small, deep holes in the surface that only appear on the magnetically coated side of the tape. The typical spacing of these defects is $\sim 10 \mu\text{m}$, with the more prominent ones being $50 - 100 \mu\text{m}$ apart. It seems most likely that these are formed during manufacture, perhaps by small bubbles emerging from the glue. Whatever their cause, such defects in the magnetic film would be expected to lead to precisely the kind of structure that we observe in our cold atom clouds.

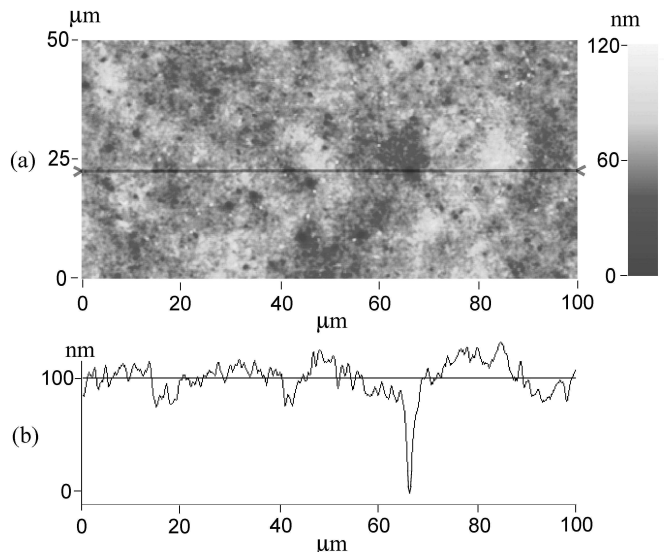


FIG. 10: Atomic force microscope scan showing topography of a piece of videotape. (a) Survey of a $100 \mu\text{m} \times 50 \mu\text{m}$ region. (b) Height versus position along the line indicated in (a).

VI. CONCLUSION AND PROSPECTS

We have shown how to load cold atoms into microtraps formed by patterns of magnetisation on videotape and we have used these clouds to demonstrate a basic understanding of the magnetic field and the traps above the tape. The videotape is well suited to making very anisotropic traps, which are of interest in the study of one-dimensional quantum gases. Indeed, we have made traps with an aspect ratio as large as $40 \text{ kHz} \times 4 \text{ Hz}$. With this in mind, we have cooled the atom clouds down to $1 \mu\text{K}$ and have studied the smoothness of the trapping potentials formed by the videotape. This experiment shows no undesirable structure within the trap at a distance of $100 \mu\text{m}$ (where $f_r \leq 1 \text{ kHz}$), but reveals microscopic wells of order $1 \mu\text{K}$ deep at a distance of $50 \mu\text{m}$ (where $f_r \leq 10 \text{ kHz}$). We have identified that this is due to physical defects in the magnetic film itself, which probably render the videotape unsuitable for the study of 1D gas in smooth traps with the highest radial frequencies. However, the method of writing magnetic patterns on videotape remains a versatile and promising technique for manipulating the atoms $100 \mu\text{m}$ away from the surface. At present we are installing optical fibres on the chip, which will operate at that height and will be used to investigate the interaction of light with trapped Bose-Einstein condensates [26]. Further information about the development of micro-optical components can be found in [25].

Recent research on Pt/Co multilayer thin films [8] appears to offer a solution to the problem of homogeneity of the magnetic layer. A pattern of lines with $2 \mu\text{m}$ period has been written on this material and the result indicates that the field should be exceedingly smooth at heights

above a few micrometers. With these films we anticipate using the techniques developed in this paper to prepare one-dimensional gases in extremely elongated traps.

In conclusion, we have shown that cold atoms can be loaded into micro-traps formed above a videotape, thereby demonstrating a first rudimentary permanent-magnet atom chip.

Acknowledgments

We are indebted to Alan Butler, Jon Dyne and Bandu Ratnasekara for technical assistance. This work is sup-

ported by the UK Engineering and Physical Sciences Research Council, the Royal Society, and the FASTnet and QGates networks of the European Union.

-
- [1] T. M. Roach, H. Able, M. G. Boshier, H. L. Grossman, K. P. Zetie, and E. A. Hinds, *Phys. Rev. Lett.* **75**, 629 (1995).
 - [2] I. G. Hughes, P. A. Barton, T. M. Roach, M. G. Boshier, and E. A. Hinds, *J. Phys. B: At. Mol. Opt. Phys.* **30**, 647 (1997).
 - [3] I. G. Hughes, P. A. Barton, T. M. Roach, and E. A. Hinds, *J. Phys. B: At. Mol. Opt. Phys.* **30**, 2119 (1997).
 - [4] C. V. Saba, P. A. Barton, M. G. Boshier, I. G. Hughes, P. Rosenbusch, B. E. Sauer, and E. A. Hinds, *Phys. Rev. Lett.* **82**, 468 (1999).
 - [5] P. Rosenbusch, B. V. Hall, I. G. Hughes, C. V. Saba, and E. A. Hinds, *Phys. Rev. A* **61**, 031404(R) (2000).
 - [6] P. Rosenbusch, B. V. Hall, I. G. Hughes, C. V. Saba, and E. A. Hinds, *Appl. Phys. B* **70**, 709 (2000).
 - [7] D. C. Lau, R. J. McLean, A. I. Sidorov, D. S. Gough, J. Koperski, W. J. Rowlands, B. A. Sexton, G. I. Opat, and P. Hannaford, *Journal of Optics B: Quantum and Semiclassical Optics* **1**, 371 (1999).
 - [8] S. Eriksson, F. Ramirez-Martinez, E. A. Curtis, B. E. Sauer, P. W. Nutter, E. W. Hill, and E. A. Hinds, *Appl. Phys. B* **79**, 811 (2004).
 - [9] I. Barb, R. Gerritsma, Y. T. Xing, J. B. Goedkoop, and R. J. C. Spreeuw, *arXiv:physics/0501109* (2005).
 - [10] B. Lev, Y. Lassailly, C. Lee, A. Scherer, and H. Mabuchi, *Appl. Phys. Lett.* **83**, 395 (2003).
 - [11] R. Folman, P. Krueger, J. Schmiedmayer, J. Denschlag, and C. Henkel, *Advances in Atomic, Molecular, and Optical Physics* **48**, 236 (2002).
 - [12] J. Reichel, *Appl. Phys. B* **75**, 469 (2002).
 - [13] P. D. D. Schwindt, S. Knappe, V. Shah, L. Hollberg, and J. Kitching, *Appl. Phys. Lett.* **85**, 6409 (2004).
 - [14] E. A. Hinds, C. J. Vale, and M. G. Boshier, *Phys. Rev. Lett.* **86**, 1462 (2001).
 - [15] P. Treutlein, P. Hommelhoff, T. Steinmetz, T. W. Hänsch, and J. Reichel, *Phys. Rev. Lett.* **92**, 203005 (2004).
 - [16] S. Knappe, V. Shah, P. D. D. Schwindt, L. Hollberg, J. Kitching, L.-A. Liew, and J. Moreland, *Appl. Phys. Lett.* **85**, 1460 (2004).
 - [17] E. A. Hinds and I. G. Hughes, *J. Phys. D: Appl. Phys.* **32**, R119 (1999).
 - [18] S. A. Hopkins, E. A. Hinds, and M. G. Boshier, *Appl. Phys. B* **73**, 51 (2001).
 - [19] R. P. Bertram, H. Merimeche, M. Mützel, H. Metcalf, D. Haubrich, D. Meschede, P. Rosenbusch, and E. A. Hinds, *Phys. Rev. A* **63**, 053405 (2001).
 - [20] J. A. Retter, Ph.D. thesis, University of Sussex (2002).
 - [21] J. Reichel, W. Hänsel, and T. W. Hänsch, *Phys. Rev. Lett.* **83**, 3398 (1999).
 - [22] Z. T. Lu, K. L. Corwin, M. J. Renn, M. H. Anderson, E. A. Cornell, and C. E. Weiman, *PRL* **77**, 3331 (1996).
 - [23] J. Fortagh, H. Ott, S. Kraft, A. Guenter, and C. Zimmermann, *PRA* **66**, 041604 (2002).
 - [24] M. P. A. Jones, C. J. Vale, D. Sahagun, B. V. Hall, C. C. Eberlein, B. E. Sauer, K. Furusawa, D. Richardson, and E. A. Hinds, *J. Phys. B: At. Mol. Opt. Phys.* **37**, L15 (2004).
 - [25] S. Eriksson, M. Trupke, H. F. Powell, D. Sahagun, C. D. J. Sinclair, E. A. Curtis, B. E. Sauer, E. A. Hinds, Z. Maktadir, C. O. Gollasch, and M. Kraft, *arXiv:physics/0502031* (2005).
 - [26] A paper reporting Bose-Einstein condensation on this atom chip is in preparation.